Article

EPR Spectra of Sintered $Cd_{1-x}Cr_xTe$ Powdered Crystals with Various Cr Content

Ireneusz Stefaniuk [1],*[ID], Werner Obermayr [2], Volodymyr D. Popovych [3], Bogumił Cieniek [1][ID] and Iwona Rogalska [1]

1   College of Natural Sciences, University of Rzeszow, Rejtana 16a, 35-310 Rzeszow, Poland; bcieniek@ur.edu.pl (B.C.); iwrogalska@ur.edu.pl (I.R.)
2   Institute for Electronic Engineering, FH Joanneum, Alte Poststraße 147, 8020 Graz, Austria; werner.obermayr@fh-joanneum.at
3   Department of Machine Science and Fundamental Technologies, Ivan Franko Drogobych State Pedagogical University, Ivan Franko Str. 24, 82100 Drogobych, Ukraine; v.popovych@dspu.edu.ua
*   Correspondence: istef@ur.edu.pl

Abstract: In this paper, we show a simple method of producing ferromagnetic materials with a Curie temperature above room temperature. The electron paramagnetic resonance (EPR) spectra of $Cd_{1-x}Cr_xTe$ (0.002 < x < 0.08) were measured with a dependence on temperature (82 K < T < 381 K). Obtained EPR lines were fitted to a Lorentz-shaped curve. The temperature dependencies of the parameters of the EPR lines, such as the peak-to-peak linewidth (H_{pp}), the intensity (A), as well as the resonance field (H_r), were studied. Ferromagnetism was noticed in samples at high temperatures (near room temperature). For a sample with a nominal concentration of chrome of x = 0.05, a very strong intrinsic magnetic field is observed. The value of the effective gyromagnetic factor for this sample is g_e = 30 at T = 240 K. An increase of chrome concentration above x = 0.05 reduces the ferromagnetic properties considerably. Analysis of the temperature dependencies of the integral intensity of EPR spectra was carried out using the Curie–Weiss law and the paramagnetic Curie temperature was obtained.

Keywords: diluted magnetic semiconductors; CdTe:Cr; ferromagnetic materials; electron paramagnetic resonance; Curie temperature

1. Introduction

Diluted magnetic semiconductors (DMSs) are of interest, mainly due to the spin–spin exchange interaction between the localized magnetic moments and the band electrons [1,2]. This property of DMS material has potential applications in spin-dependent semiconductor electronics for information processing (spintronics) [3–6].

A substantial amount of work has been done on Mn-based DMSs. Ferromagnetism has been discovered in materials comparable with the semiconductors used in present electronics, like as (In, Mn)As [7], (Ga, Mn)As [8], Mg [9,10], and $Cd_{1-x}Mn_xTe$ [11–13]. Ferromagnetic properties in DMS make them basic component for spintronics. However, their Curie temperatures (T_C) (e.g., 110 K for (Ga, Mn)As [14]) are not high enough for real applications.

The ferromagnetism in DMS has also been investigated theoretically using a model Hamiltonian [15–17]. Dietl et al. proposed Zener's p–d exchange interaction to describe magnetism [15,16]. This model predicts room-temperature ferromagnetism (RTFM) in (Ga, Mn)N [15,16]. Liu et al. confirmed the ferromagnetic character of the p–d exchange interaction in Cr-based II-VI DMSs [18,19]. Blinowski et al. [20] pointed out very interesting properties of Cr-based DMS and predicted ferromagnetism at room temperature in CdTe:Cr. In the last few years, Cr-doped II-VI DMS compounds have been studied extensively to determine improved ferromagnetic properties and to explore the mechanism behind the half-metallic ferromagnetism (HMF) [21–28].

Some earlier experiments for semiconductor CdTe with Cr using the EPR method were performed. Ludwig and Lorentz [29] studied Cr^{1+} ($3d^5$) ions substituted into the cadmium sites in CdTe using electron nuclear double resonance (ENDOR) and EPR. Chromium ions substituting for cadmium ions are expected to be in the Cr^{2+} valence state, i.e., in the $3d^4$ configuration. However, the authors of [29] determined the total spin S = 5/2, g = 1.9997 ± 0.0003, as well the parameters of the cubic zero-field splitting and the hyperfine interaction with second neighbors Cd^{111} and Cd^{113}. Vallin and Watkins [30] investigated the EPR spectra of Cr^{2+} in CdTe. The Jahn–Teller coupling coefficients from the changes of the fine structure of the EPR spectra under uniaxial stress were determined. Stefaniuk et al. [31] studied the fine structure of Cr^{3+} ions in CdTe:Cr. The EPR spectra also contained a very broad line assigned to Cr^{2+} ions in CdTe, which are related to magnetic interactions [31,32]. Magnetic properties of Cr-based DMS were studied by Mac et al. [33] and Ko and Blamire [34,35]. Many experiments have been performed to search for DMSs with RTFM and, recently, high T_C values have been reported for several systems, e.g., (Ga, Mn)N [36–38] (Ga, Cr)N [39], and (ZnCr)Te [40–42].

There is a large group of materials with ferromagnetic properties, with a Curie temperature above 500 K (see [43]). However, the goal of this work is to obtain a ferromagnetic semiconductor (DMS) meeting the needs of spintronics.

In this paper, we investigate $Cd_{1−x}Cr_xTe$ powdered bulk crystals that were doped with different concentrations of chrome (up to x = 0.08) during the synthesis process. A wide temperature range of crystals was studied using the EPR method. This study aims to determine the optimal content of Cr ions at which ferromagnetic properties are observed at room temperature.

2. Materials and Methods

The crystal preparation procedure consisted of two subsequent stages: the synthesis of polycrystalline source and a crystal growth process, described in more detail in other work [44]. High purity elemental CdTe (99.9999%) supplied by Alfa Aesar and also Cr_2Te_3 powder with particle sizes under 325 mesh (99.96%) from Sigma-Aldrich (Saint Louis, MO, USA) were used for (Cd,Cr)Te synthesis. The calculation of the appropriate constituent weights was done considering that chromium atoms substitute cadmium ones and a $Cd_{1−x}Cr_xTe$ solid solution was formed. We studied the pulverized $Cd_{1−x}Cr_xTe$ crystals doped with different nominal concentrations of chrome (up to x = 0.08) during the synthesis process. Growth temperatures were in the range of 1280–1320 °C. The final materials were solid solutions of the source components. The chromium concentrations in the samples were measured by X-ray energy dispersive fluorescent analysis (XFA) (Table 1). All samples for EPR studies were pulverized in an agate mortar. To investigate the crystal structure of samples X-ray diffraction (XRD) was used.

Table 1. Samples investigated.

Sample	Growth Temperature, °C	The Concentration of Cr in $Cd_{1−x}Cr_xTe$	
		Charge, x	XFA Measurement, x
1p	1280	0.04	0.002
2p	1300	0.01	0.008
3p	1300–1310	0.05	0.04
4p	1320	0.05	0.05
5p	1320	0.1	0.08

The EPR measurements were performed on an X-band (~9 GHz) spectrometer with a digital registration of the spectra. Part of the EPR measurements was performed on an EPR spectrometer (Bruker multifrequency and multiresonance FT-EPR ELEXSYS E580, Bruker Analytische Messtechnik, Rheinstetten, Germany). The temperature measurements using the digital temperature control system (Bruker ER 4131VT) in the temperature range from 82–381 K were done.

3. Results

The EPR spectra are presented in Figures 1–5. In every sample, we observed a wide EPR signal which, however, is irregular for low concentrations of chrome (sample 1p and 2p). In samples 1p and 2p, as well as in sample 5p, we observed a small shift in the EPR line towards a higher magnetic field with increasing temperature. For samples 3p and 4p, very regular shapes of the EPR spectra above room temperature (Figures 3 and 4) were obtained. At lower temperatures, the resonance field shifted towards lower magnetic fields, and then only a part of the EPR line was observed. The EPR lines presented in Figures 1–5 are arranged such that they are shifted upwards with increasing temperature, as indicated by the legend. The amplitudes of the EPR signals for samples 1p, 2p, and 3p became smaller when the temperature was lowered from room temperature. However, for samples 4p and 5p, we first observed an increase in the amplitude of the signal with reduced temperature, but below a certain temperature a decrease was noted. Furthermore, the linewidth strongly depended on both, the temperature and the sample, i.e., the concentration of chromium.
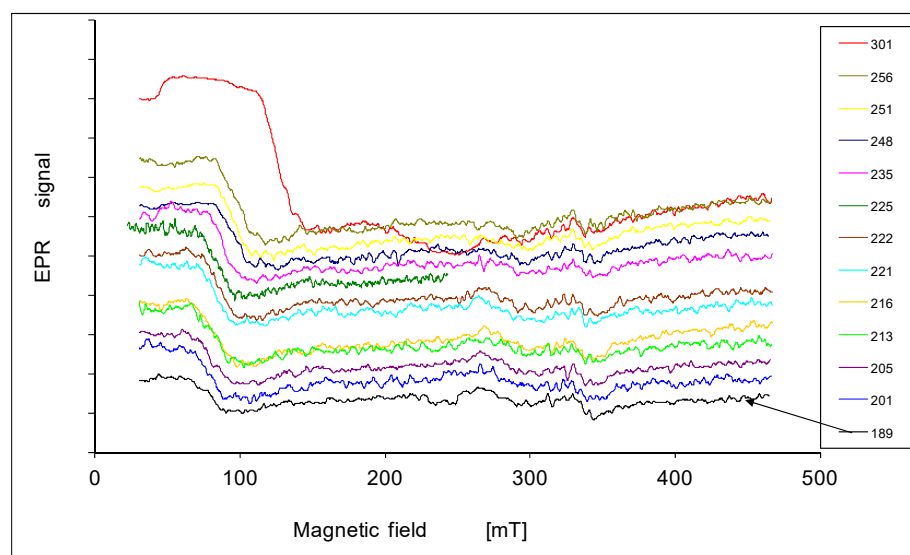

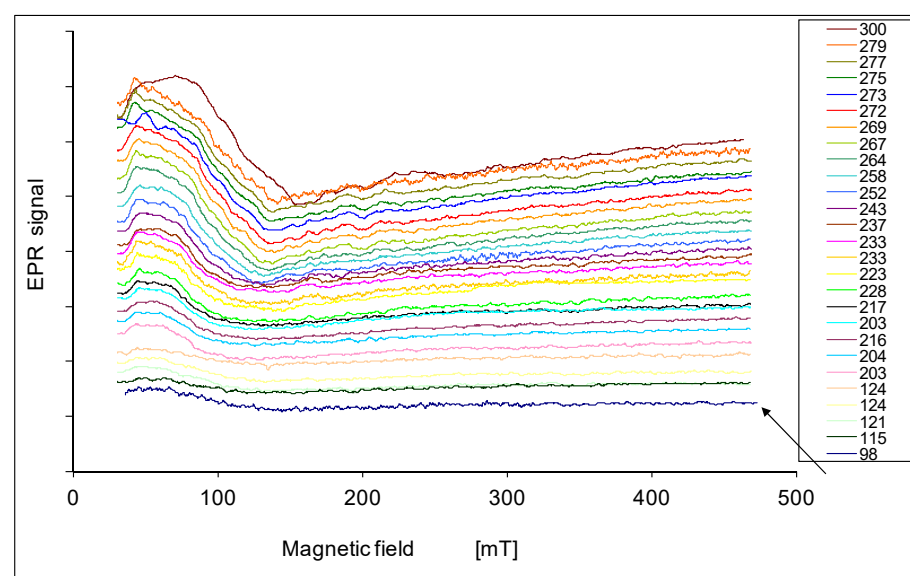**Figure 1.** EPR spectra of the sample 1p at various temperatures in K.

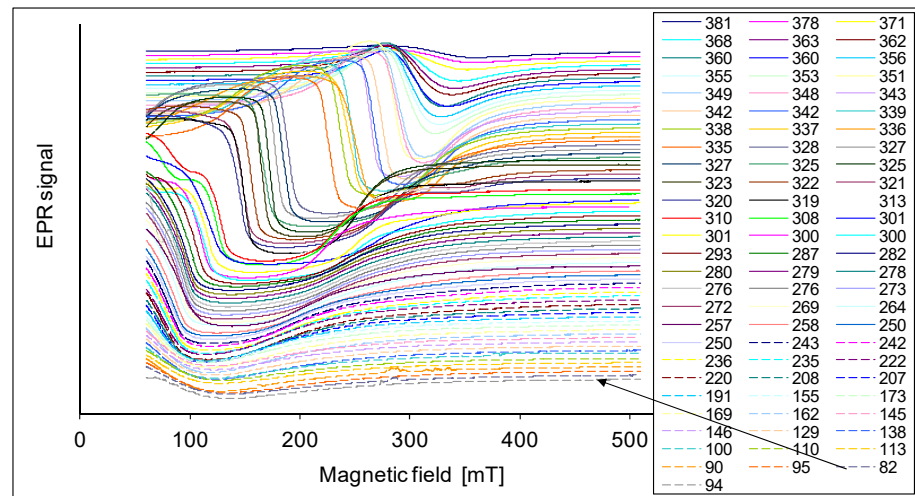**Figure 2.** EPR spectra of the sample 2p at various temperatures in K.

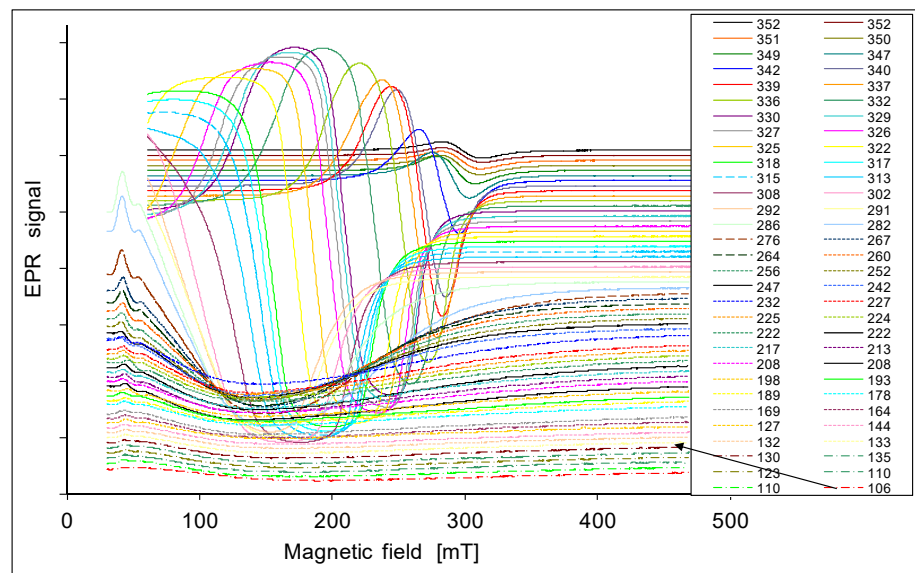**Figure 3.** EPR spectra of the sample 3p at various temperatures in K.

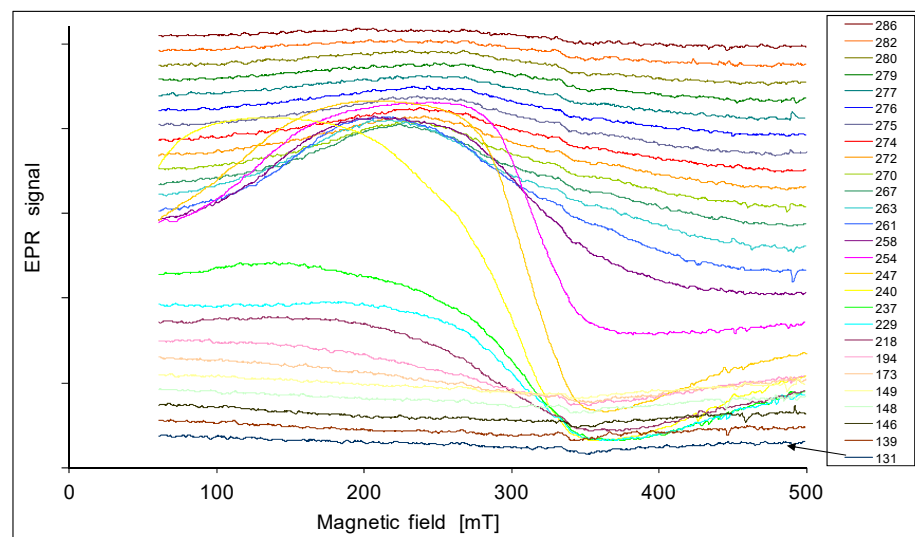**Figure 4.** EPR spectra of the sample 4p at various temperatures in K.

Figure 5. EPR spectra of the sample 5p at various temperatures in K.

4. Discussion

The ferromagnetic properties of semiconductors are the subject of wide investigations at present. It is known that for similar materials, the shape of an EPR line is closely related to the kind of magnetic interaction [45–49]. Since the exact mechanisms of ferromagnetism in the present material are still not known, the choice of the theoretical curve for the fitting of the experimental data is not straightforward. Therefore, in the initial stage of the research, we focused on the determination of the appropriate concentration of chromium, depending on strong ferromagnetic properties at high temperatures. This was realized by measurements of the temperature dependences of the peak-to-peak linewidth H_{pp}, the peak amplitude A, and the resonance field H_r. The latter is in simple relation to the effective gyromagnetic factor g_e. Since the majority of the measured EPR spectra are not complete due to the large linewidth and their shifts towards smaller magnetic fields for lower temperatures, it is impossible to get the line parameters directly from the spectra. Thus, these parameters were determined by fitting the resonance line to the theoretical curve by using the standard computer program OriginPro 7.5, OriginLab, Northampton, MA, USA. For numerical analysis, a Lorentzian function was applied [50],

$$y = P - \frac{3^{\frac{1}{2}} \times H_{pp} \times (\chi - H_r)}{\pi \times \left(0.75 \times H_{pp}^2 + (\chi - H_r)^2\right)^2} \times A \tag{1}$$

where P is a constant, H_{pp} is the peak-to-peak-width, H_r is the resonance field, and A is the peak amplitude. The analysis of the shape of the experimental line shows its complex structure. In this work, we used fitting with a single Lorentz shape line as the closest match to the real one. We are aware that some parameters are different (e.g., intensity of line A), but, at the same time, other parameters are obtained with good accuracy (e.g., resonance field H_r).

As an example, in Figure 6, we show the result of the fitting of an experimental spectrum to a Lorentzian curve. As it is shown in Figure 6b for the incomplete EPR lines very well-fitting results were received. However, the fitting to the whole or considerable parts of the visible lines as one can see in Figure 6a was worse. For example, the accuracy of the fitting for a small number of some very irregular lines, the EPR spectrum of the sample 5p at the temperature around 240 K, was poor. The value of the resonance field H_r is very well reproduced, whereas the linewidth H_{pp} shows deviations up to maximal errors of several percent. However, we are interested in the temperature dependence of H_{pp}. From such diagrams, we are able with good accuracy to find the temperature in which the large changes of H_{pp} occur.
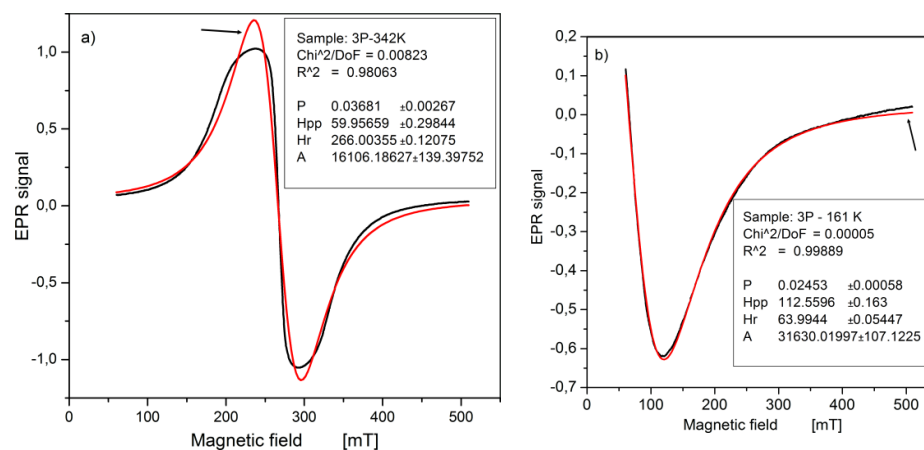

Figure 6. Representative EPR spectra of $Cd_{1-x}Cr_xTe$ powdered crystals: (**a**) sample No. 3p at T = 342 K, (**b**) sample No 3p at T = 161 K. The arrow marks the theoretical line. The fitting parameters are given in the legend.

Determining parameters of the EPR spectra such as H_r (or g_e), H_{pp}, and A, are presented in Figures 7–9. In Figure 7 the temperature dependence of the effective gyromagnetic factor g_e is shown for all samples. In a paramagnetic material, the applied external Zeeman field is equal to the local field and the g-factor is obtained from the Zeeman formula. The effect is more complicated in ferromagnets. The local resonance field is a superposition of the external field H_0, the demagnetizing field, and other contributions to the magnetic anisotropy energy [49,51]. We observe a paramagnetic phase at higher temperatures with g_e close to 2. However, at lower temperatures, the value of g_e increases due to intrinsic magnetic fields responsible for ferromagnetism. A larger value of g_e is related to a larger intrinsic magnetic field. The samples 1p and 2p with small concentrations of chrome show ferromagnetic properties with g_e about 8. With the increase of the concentration of chrome as in sample 3p, an increase of g_e ($g_e = 10$) was observed. In sample 4p it accepts a very large value close to $g_e = 30$. This is a very high value in comparison with other materials. Further increase of concentration like in the sample 5p, an interesting effect is seen, that g_e again accepts the value of about 2. A possible explanation may be the appearance of antiferromagnetic interactions. Similar results have been found for Mn in $CaMn_{1-x}Ru_xO_3$ [47].

In Figure 8, we show the temperature dependence of linewidth. For the samples 1p, 2p, and 3p, we find a maximum for H_{pp} approximately at room temperature. For sample 4p the maximum is found close to 170 K. However, for sample 5p the linewidth increases with lower temperatures. In the samples 2p and 3p, the linewidth remains almost constant below 160 K. For the samples 3p and 4p we observe a decrease of the linewidth when the temperature is raised above room temperature, and we get a minimum for H_{pp} in the range 340–350 K. For higher temperatures we find an increase of the linewidth again and simultaneously a reduction of the intensity; this is the typical behavior of a paramagnetic sample [49]. The largest change of the linewidth H_{pp} in dependence of the temperature is in the sample 4p: it changes from 25 mT at 346 K to 250 mT at 180 K.
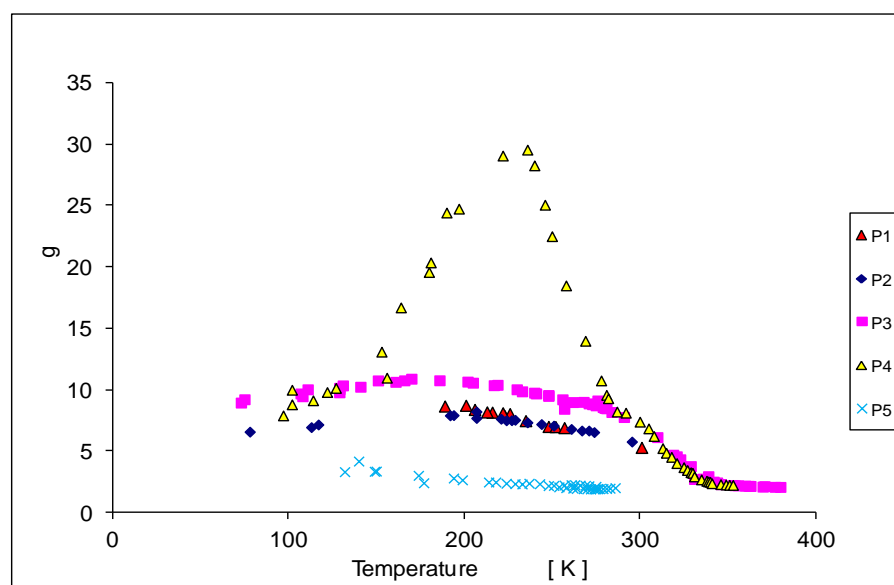

Figure 7. The temperature dependence of the effective gyromagnetic factor g_e.
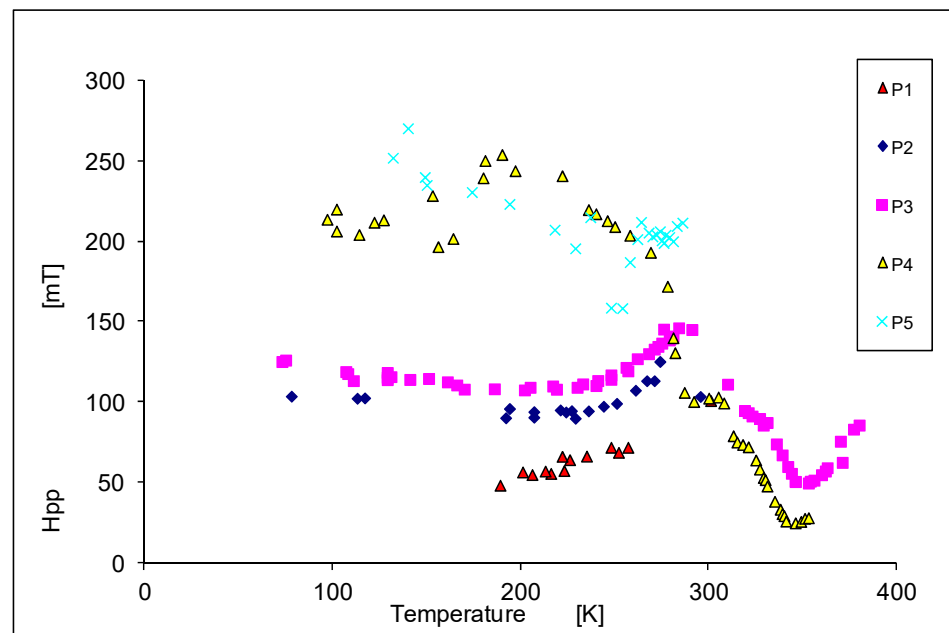
Figure 8. The temperature dependence of the peak-to-peak linewidth (H_{pp}).
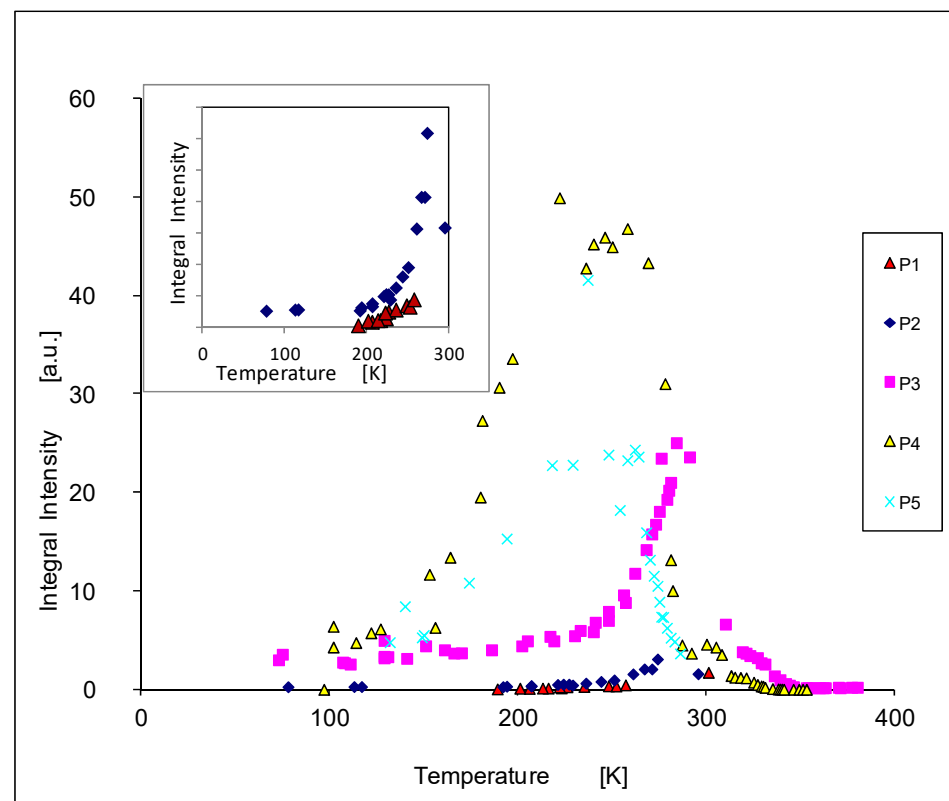

Figure 9. The temperature dependence of the integral intensity I_t ($I_t = A \times H_{pp}^2$).

The temperature dependence of the integral intensity is shown in Figure 9. We see that for the samples with higher concentrations of chrome the maxima of the intensities are shifted to lower temperatures. Furthermore, we observe that the intensities rise with increasing concentrations of chrome (samples 1p, 2p 3p); the maximum is obtained for the sample 4p, and then it decreases again like in sample 5p.

The presented results were completed by studies of the chemical and crystallographic homogeneity of the samples. For this aim, we performed XRD measurements. The spectra

of our samples were compared with those of pure CdTe as well as with CrTe phases such as Cr_7Te_8, Cr_3Te_4, Cr_5Te_6, etc. which are the most likely inclusions of the second phase (Cr_2Te_3 was an initial component in the process of the CdCrTe synthesis). In Figure 10 spectra with those given by standard ASTM X-ray powder data were compared. The main diffraction peaks of our sample no. 4p (Figure 10f) corresponds very well with the zinc-blende structure of the CdTe crystal (Figure 10d,e). We have not detected diffraction peaks from CrTe phases which crystallize in a different structure—in the structure of NiAs [52] (see Figure 10a–c).
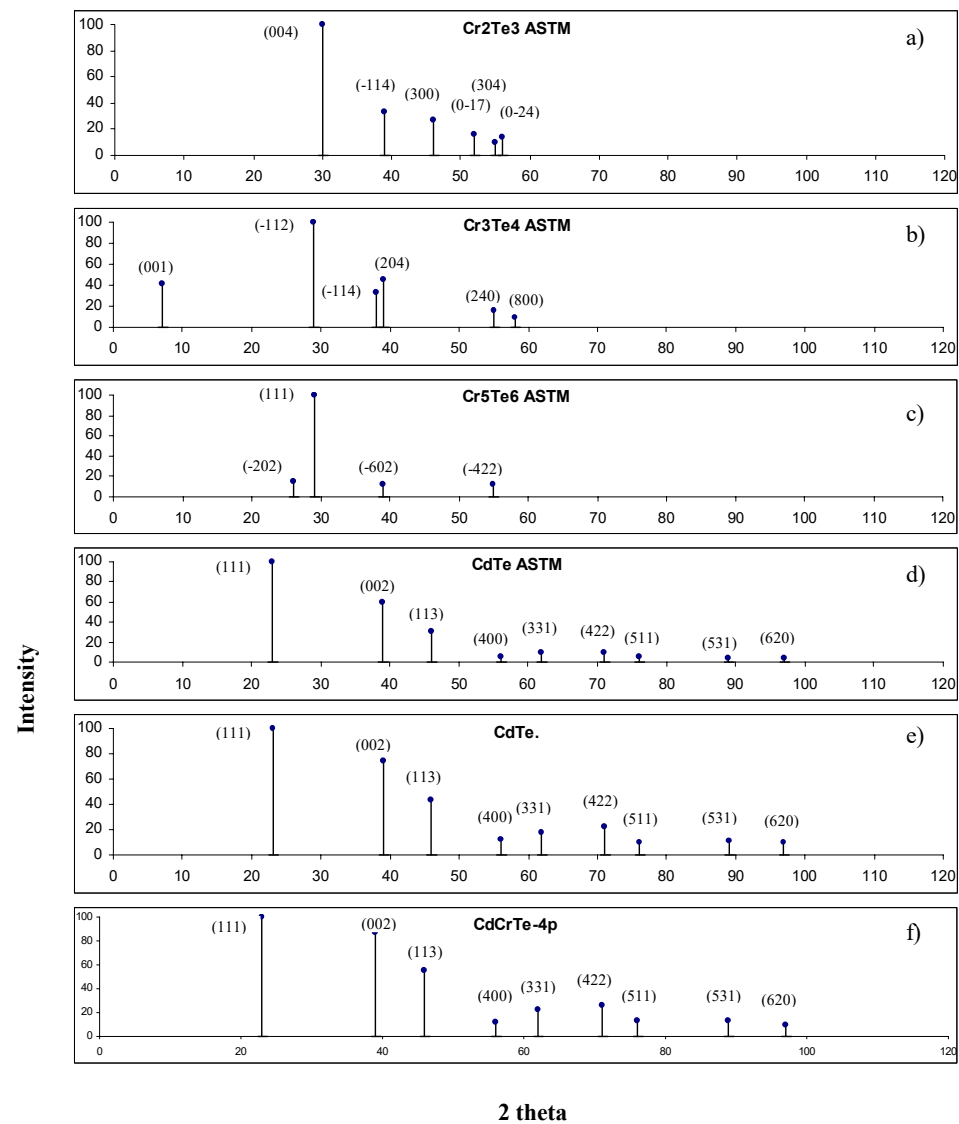

Figure 10. XRD spectra of CrTe, CdTe, (**a–d**)—according to the ASTM tables, and CdTe, CdCrTe (**e,f**)—experimental results.

The lack of the second phase in our samples is also demonstrated by the EPR measurements of the Cr_2Te_3 powder (the initial material for CdCrTe synthesis), as well as of the Cr_2Te_3 solid (premelted in the conditions of CdCrTe synthesis). These spectra for the temperature of 260 K are shown in Figure 11. They also differ considerably from those obtained for CdCrTe. The resonance fields are 341 mT and 347 mT for powdered and solid Cr_2Te_3, respectively, whereas for CdCrTe it has a value of 95 mT. The EPR line of Cr_2Te_3 at room temperature (paramagnetic phase) is also of Lorentzian shape, however, with decreasing temperature the shape changes towards a Dysonian function, particularly at

low temperatures. The positions of the lines (of Cr_2Te_3 powdered and solid) do not change with temperature contrary to the EPR line of CdCrTe.
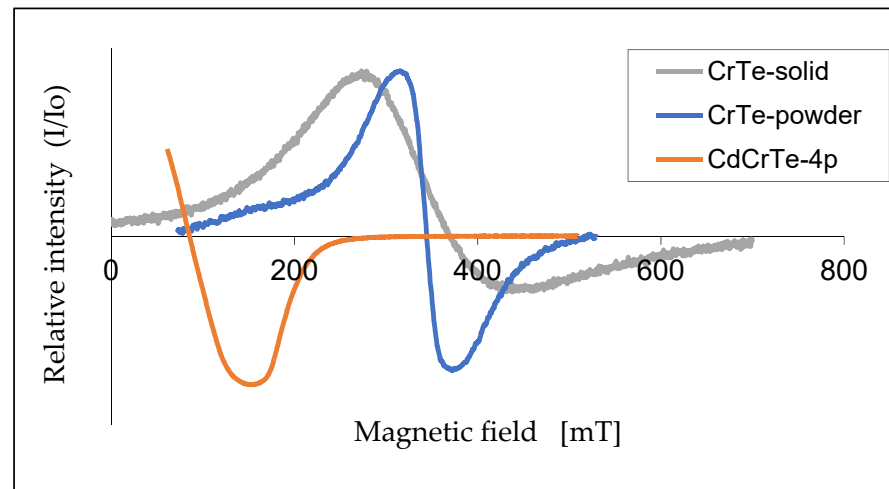

Figure 11. EPR spectra of powered, solid Cr_2Te_3, and the sample 4p (T≈260 K).

We used the Curie–Weiss law to analyze the temperature dependences of the integral intensity, which is directly proportional to the magnetic susceptibility χ. A linear increase of χ^{-1} (T) at higher temperatures can be fitted to the Curie-Weiss law [53,54],

$$(\chi - \chi_0)^{-1}(T) = (T - \theta_{cw})/C, \tag{2}$$

where C is the Curie constant, θ_{cw} is the paramagnetic Curie temperature, and χ_0 is a temperature-independent term to account for the diamagnetic host and any Pauli paramagnetism contribution. Figure 12 displays the temperature dependence of the quantity $(\chi - \chi_0)^{-1}$ for sample 4p. The lines are linear extrapolations illustrating the ferromagnetic (positive) Curie–Weiss temperatures. Fitting yields the following values: for sample 4p-θ(x) = 338.3 K and C(x) = 5.91 × 10^{-7}; for sample 3p-θ(x) = 333 K and C(x) = 7.51 × 10^{-6}; for sample 2p-θ(x) = 250 K and C(x) = 6.25 × 10^{-9}. The Curie constant has a dimension of $\frac{Km^3}{kg}$.
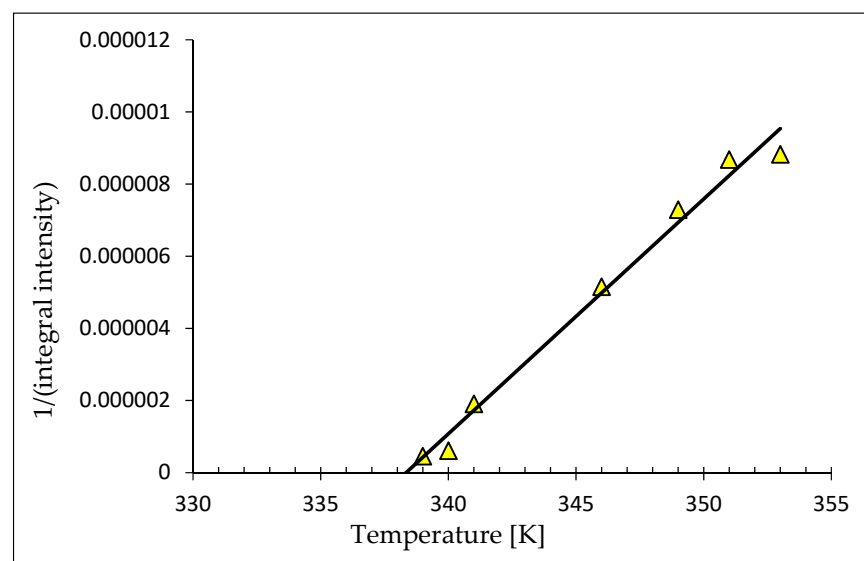

Figure 12. Temperature dependence of the 1/(integral intensity) of the sample 4p.

Ko et al. [34,35] reported a Curie temperature for a bulk Cr-doped CdTe crystal of T_C = 354 K for x = 0.06, which agrees well with our observations (Figures 7–9) and Curie temperature T_C = 338.3 K for sample 4pg_e values for the samples 3p, 4p, and 5p show small differences in the region of higher temperatures (paramagnetic region). A similar effect was observed by Son et al. [46] for Mn in $Cd_{1-x}Mn_xTe$.

A very large g_e factor (up to 30) observed for the 4p sample, shows a very strong intrinsic magnetic field, which, together with a high Curie temperature may have its origin in a superexchange interaction of Cr ions in the Cr-dissolved CdTe phase. The observed effects may indicate superparamagnetism [55–57].

5. Conclusions

The fine structure of the spectra only in the sample with a low concentration of Cr atoms (sample 1p, Figure 1) is visible. It is superimposed on the one intensive line positioned at a lower magnetic field.

In the samples with a concentration of Cr from x = 0.002 to 0.08, a broad line in the EPR spectrum is observed. The shape of this line is symmetric and regular for samples 3p and 4p. The position of the line strongly depends on the temperature.

At several characteristic temperatures, a change of the slope of the temperature depends on the resonance field (H_r), the linewidth (H_{pp}), and the total intensity (I_t) was observed. At about 160 K this is seen for H_{pp}, I_t, and especially for the g_e factor to the different range and depending on the Cr concentration; at 240 K for the $g_e(T)$ dependence especially in sample 4p; at 280 K (room temperature) for $H_{pp}(T)$ in all samples, and to a smaller extent for $g_e(T)$ and $I_t(T)$; in the temperature range 340–350 K for H_{pp}, g_e, and I_t in the samples 3p and 4p.

g_e values for the samples 3p, 4p, and 5p show small differences in the region of higher temperatures (paramagnetic region). The value of g_e is higher for larger concentrations of Mn. However, we obtained the values 2.18, 2.28, and 1.93 for the samples 3p, 4p, and 5p, respectively. Thus, g_e does not shift to higher values with increasing concentration of Cr but achieves a maximum for x = 0.05 (sample 4p).

The most interesting magnetic properties for the sample 4p in the vicinity of room temperature, for all EPR line parameters, were observed. A very large g_e factor (up to 30) shows a very strong intrinsic magnetic field. This intrinsic ferromagnetism together with a high Curie temperature may have its origin in a superexchange interaction of Cr ions in the Cr-dissolved CdTe phase. The observed effects indicate possible superparamagnetism. Detailed research for this sample will be conducted further, especially taking into account the precise analysis of the line shape, as well as the registration of the spectrum in the negative field. The use of a simple method of sintered powdered materials: Cd, Te, and Cr_2Te_3 allows for easy control of the content of chromium ions in $Cd_{1-x}Cr_xTe$. The DMS obtained in this way shows ferromagnetic properties at room temperature, especially in the range x = 0.05–0.1.

It is found that an increase of the concentration of Cr up to x = 0.05 enlarges the ferromagnetic properties, but a further augmentation of the Cr concentration reduces ferromagnetism and may lead to the presence of antiferromagnetism.

Institutional Review Board Statement: Not applicable.

Informed Consent Statement: Not applicable.

Data Availability Statement: Data sharing is not applicable to this article.

Conflicts of Interest: The authors declare no conflict of interest.

References

1. Dobrowolski, W.; Kossut, J.; Story, T. II-VI and IV-VI Diluted Magnetic Semiconductors—New Bulk Materials and Low-Dimensional Quantum Structures. *Handb. Magn. Mater.* **2003**, *15*, 289–377.
2. Kacman, P. Spin interactions in diluted magnetic semiconductors and magnetic semiconductor structures. *Semicond. Sci. Technol.* **2001**, *16*, R25–R39. [CrossRef]
3. Awschalon, D.D.; Loss, D. *Semiconductors Spintronics and Quantum Computation*; Springer: Berlin/Heidelberg, Germany, 2002; ISBN 9783642075773.
4. Ohno, H. Making nonmagnetic semiconductors ferromagnetic. *Science* **1998**, *281*, 951–956. [CrossRef] [PubMed]
5. Wolf, S.A.; Awschalom, D.D.; Buhrman, R.A.; Daughton, J.M.; Von Molnár, S.; Roukes, M.L.; Chtchelkanova, A.Y.; Treger, D.M. Spintronics: A spin-based electronics vision for the future. *Science* **2001**, *294*, 1488–1495. [CrossRef]
6. Laref, A.; AlMudlej, A.; Laref, S.; Yang, J.T.; Xiong, Y.C.; Luo, S.J. Ab-initio investigations of magnetic properties and induced half-metallicity in $Ga_{1-x}Mn_xP$ (x = 0.03, 0.25, 0.5, and 0.75) Alloys. *Materials* **2017**, *10*, 766. [CrossRef]
7. Ohno, H.; Munekata, H.; Penney, T.; Von Molnar, S.; Chang, L.L. Magnetotransport properties of p-type (In,Mn)As diluted magnetic III–V semiconductors. *Phys. Rev. Lett.* **1992**, *68*, 2664–2667. [CrossRef] [PubMed]
8. Ohno, H.; Shen, A.; Matsukura, F.; Oiwa, A.; Endo, A.; Katsumoto, S.; Iye, Y. (Ga,Mn)As: A new diluted magnetic semiconductor based on GaAs. *Appl. Phys. Lett.* **1996**, *69*, 363–365. [CrossRef]
9. Yu, P.; Jiang, B.; Chen, Y.; Zheng, J.; Luan, L. Study on In-Doped CdMgTe Crystals Grown by a Modified Vertical Bridgman Method Using the ACRT Technique. *Materials* **2019**, *12*, 4236. [CrossRef] [PubMed]
10. Yavorskiy, D.; Szoła, M.; Karpierz, K.; Rudniewski, R.; Bozek, R.; Karczewski, G.; Wojtowicz, T.; Wróbel, J.; Łusakowski, J. Polarization of magnetoplasmons in grating metamaterials based on CdTe/CdMgTe quantum wells. *Materials* **2020**, *13*, 1811. [CrossRef]
11. Furdyna, J.K.; Kossut, J. *Semiconductors and Semimetals*; Willardson, R.K., Beer, A.C., Eds.; Academic Press, Inc.: Cambridge, MA, USA, 1988; Volume 25, ISBN 9780080864228.
12. Sayad, H.A.; Bhagat, S.M. Dynamic random fields in diluted magnetic semiconductors: $Cd_{1-x}Mn_xTe$. *Phys. Rev. B* **1985**, *31*, 591–593. [CrossRef]
13. Oseroff, S.B. Magnetic susceptibility and EPR measurements in concentrated spin-glasses: $Cd_{1-x}Mn_xTe$ and $Cd_{1-x}Mn_xSe$. *Phys. Rev. B* **1982**, *25*, 6584–6594. [CrossRef]
14. Matsukura, F.; Ohno, H.; Shen, A.; Sugawara, Y. Transport properties and origin of ferromagnetism in (Ga, Mn)As. *Phys. Rev. B Condens. Matter Mater. Phys.* **1998**, *57*, R2037–R2040. [CrossRef]
15. Dietl, T.; Ohno, H.; Matsukura, F.; Cibert, J.; Ferrand, D. Zener Model Description of Ferromagnetism in Zinc-Blende Magnetic Semiconductors. *Science* **2000**, *287*, 1019–1022. [CrossRef]
16. Dietl, T. Ferromagnetic semiconductors. *Semicond. Sci. Technol.* **2002**, *17*, 377–392. [CrossRef]
17. Jungwirth, T.; König, J.; Sinova, J.; Kučera, J.; MacDonald, A.H. Curie temperature trends in (III,Mn)V ferromagnetic semiconductors. *Phys. Rev. B Condens. Matter Mater. Phys.* **2002**, *66*, 124021–124024. [CrossRef]
18. Lu, X.; Tsoi, S.; Miotkowski, I.; Rodriguez, S.; Ramdas, A.K.; Alawadhi, H. Raman electron paramagnetic resonance in $Zn_{1-x}Cr_xTe$ and $Cd_{1-x}Cr_xTe$. *Phys. Rev. B Condens. Matter Mater. Phys.* **2007**, *75*, 155206. [CrossRef]
19. Lu, X.; Miotkowski, I.; Rodriguez, S.; Ramdas, A.K.; Alawadhi, H.; Pekarek, T.M. Magnetization and spin-flip Raman scattering in $Cd_{1-x}Cr_xSe$ and $Cd_{1-x}V_xSe$. *Phys. Rev. B Condens. Matter Mater. Phys.* **2012**, *86*, 115213. [CrossRef]
20. Blinowski, J.; Kacman, P.; Majewski, J.A. Ferromagnetism in Cr-based diluted magnetic semiconductors. *J. Cryst. Growth* **1996**, *159*, 972–975. [CrossRef]
21. Sajjad, M.; Zhang, H.X.; Noor, N.A.; Alay-E-Abbas, S.M.; Shaukat, A.; Mahmood, Q. Study of half-metallic ferromagnetism in V-doped CdTe alloys by using first-principles calculations. *J. Magn. Magn. Mater.* **2013**, *343*, 177–183. [CrossRef]
22. Amari, S.; Méçabih, S.; Abbar, B.; Bouhafs, B. Half-metallic ferromagnetism in ZnCrTe and CdCrTe: Ab initio study. *Comput. Mater. Sci.* **2011**, *50*, 2785–2792. [CrossRef]
23. Ge, X.F.; Zhang, Y.M. First-principles study of half-metallic ferromagnetism in $Zn_{1-x}Cr_xSe$. *J. Magn. Magn. Mater.* **2009**, *321*, 198–202. [CrossRef]
24. Saito, H.; Yamagata, S.; Ando, K. Magnetoresistance in a room temperature ferromagnetic diluted magnetic semiconductor $Zn_{1-x}Cr_xTe$. *AIP J. Appl. Phys.* **2004**, *95*, 7175–7177. [CrossRef]
25. Jia, X.; Qin, M.; Yang, W. Magnetism in Cr-doped ZnS: Density-functional theory studies. *J. Phys. D. Appl. Phys.* **2009**, *42*, 235001. [CrossRef]
26. Soundararajan, D.; Mangalaraj, D.; Nataraj, D.; Dorosinskii, L.; Santoyo-Salazar, J.; Jeon, H.C.; Kang, T.W. Magnetic studies on ZnTe:Cr film grown on glass substrate by thermal evaporation method. *Appl. Surf. Sci.* **2009**, *255*, 7517–7523. [CrossRef]
27. Nazir, S.; Ikram, N.; Siddiqi, S.A.; Saeed, Y.; Shaukat, A.; Reshak, A.H. First principles density functional calculations of half-metallic ferromagnetism in $Zn_{1-x}Cr_xS$ and $Cd_{1-x}Cr_xS$. *Curr. Opin. Solid State Mater. Sci.* **2010**, *14*, 1–6. [CrossRef]
28. Noor, N.A.; Ali, S.; Shaukat, A. First principles study of half-metallic ferromagnetism in Cr-doped CdTe. *J. Phys. Chem. Solids* **2011**, *72*, 836–841. [CrossRef]

29. Ludwig, G.W.; Lorenz, M.R. Paramagnetic resonance of chromium in CdTe. *Phys. Rev.* **1963**, *131*, 601–604. [CrossRef]

30. Vallin, J.T.; Watkins, G.D. EPR of Cr^{2+} in II–VI lattices. *Phys. Rev. B* **1974**, *9*, 2051–2072. [CrossRef]

31. Stefaniuk, I.; Bester, M.; Virt, I.S.; Kuzma, M. EPR spectra of Cr in CdTe crystals. *Acta Phys. Pol. A* **2005**, *108*, 413–418. [CrossRef]

32. Stefaniuk, I.; Bester, M.; Kuzma, M. Ferromagnetic resonance in CdCrTe solid solution. *J. Phys. Conf. Ser.* **2008**, *104*, 012010. [CrossRef]

33. Mac, W.; Twardowski, A.; Eggenkamp, P.J.T.; Swagten, H.J.M.; Shapira, Y.; Demianiuk, M. Magnetic properties of Cr-based diluted magnetic semiconductors. *Phys. Rev. B* **1994**, *50*, 14144–14154. [CrossRef] [PubMed]

34. Ko, K.Y.; Blamire, M.G. Temperature dependent magnetization in Cr-doped CdTe crystals. *Appl. Phys. Lett.* **2006**, *88*, 172101. [CrossRef]

35. Ko, K.Y.; Blamire, M.G. Temperature-induced magnetic phase transition in bulk Cr-doped CdTe Crystals. *J. Korean Phys. Soc.* **2006**, *49*, 591–595.

36. Sonoda, S.; Shimizu, S.; Sasaki, T.; Yamamoto, Y.; Hori, H. Molecular beam epitaxy of wurtzite (Ga, Mn)N films on sapphire(0 0 0 1) showing the ferromagnetic behaviour at room temperature. *J. Cryst. Growth* **2002**, *237–239*, 1358–1362. [CrossRef]

37. Theodoropoulou, N.; Hebard, A.F.; Overberg, M.E.; Abernathy, C.R.; Pearton, S.J.; Chu, S.N.G.; Wilson, R.G. Magnetic and structural properties of Mn-implanted GaN. *Appl. Phys. Lett.* **2001**, *78*, 3475–3477. [CrossRef]

38. Reed, M.L.; El-Masry, N.A.; Stadelmaier, H.H.; Ritums, M.K.; Reed, M.J.; Parker, C.A.; Roberts, J.C.; Bedair, S.M. Room temperature ferromagnetic properties of (Ga, Mn)N. *Appl. Phys. Lett.* **2001**, *79*, 3473–3475. [CrossRef]

39. Hashimoto, M.; Zhou, Y.K.; Kanamura, M.; Asahi, H. High temperature (>400 K) ferromagnetism in III–V-based diluted magnetic semiconductor GaCrN grown by ECR molecular-beam epitaxy. *Solid State Commun.* **2002**, *122*, 37–39. [CrossRef]

40. Pekarek, T.M.; Luning, J.E.; Miotkowski, I.; Crooker, B.C. Magnetization and heat-capacity measurements on $Zn_{1-x}Cr_xTe$. *Phys. Rev. B* **1994**, *50*, 16914–16920. [CrossRef]

41. Pekarek, T.M.; Arenas, D.J.; Crooker, B.C.; Miotkowski, I.; Ramdas, A.K. Magnetic measurements on ferromagnetic behavior in the bulk II–VI diluted magnetic semiconductor $Zn_{1-x}Cr_xTe$. *J. Appl. Phys.* **2004**, *95*, 7178–7180. [CrossRef]

42. Saito, H.; Zayets, V.; Yamagata, S.; Ando, K. Room-temperature ferromagnetism in highly Cr-doped II–VI diluted magnetic semiconductor $Zn_{1-x}Cr_xTe$. *AIP J. Appl. Phys.* **2003**, *93*, 6796–6798. [CrossRef]

43. Dahal, J.N.; Ali, K.S.; Mishra, S.R.; Alam, J. Structural, Magnetic, and Mössbauer Studies of Transition Metal-Doped $Gd_2Fe_{16}Ga_{0.5}TM_{0.5}$ Intermetallic Compounds (TM = Cr, Mn, Co, Ni, Cu, and Zn). *Magnetochemistry* **2018**, *4*, 54. [CrossRef]

44. Popovych, V.D.; Virt, I.S.; Sizov, F.F.; Tetyorkin, V.V.; Tsybrii (Ivasiv), Z.F.; Darchuk, L.O.; Parfenjuk, O.A.; Ilashchuk, M.I. The effect of chlorine doping concentration on the quality of CdTe single crystals grown by the modified physical vapor transport method. *J. Cryst. Growth* **2007**, *308*, 63–70. [CrossRef]

45. Larson, B.E.; Ehrenreich, H. Anisotropic superexchange and spin-resonance linewidth in diluted magnetic semiconductors. *Phys. Rev. B* **1989**, *39*, 1747–1759. [CrossRef] [PubMed]

46. Son, P.K.; Heo, K.C.; Ok, C.I.; Jeen, G.S.; Kim, J.W. EPR lineshape and g-factor of $Cd_{1-x}Mn_xTe$. *J. Korean Phys. Soc.* **2000**, *37*, 287–289.

47. Shames, A.I.; Rozenberg, E.; Martin, C.; Maignan, A.; Raveau, B.; André, G.; Gorodetsky, G. Crystallographic structure and magnetic ordering in $CaMn_{1-x}Ru_xO_3$ (x $\leq$ 0.40) manganites: Neutron diffraction, ac susceptibility, and electron magnetic resonance studies. *Phys. Rev. B Condens. Matter Mater. Phys.* **2004**, *70*, 134433. [CrossRef]

48. Joshi, J.P.; Sood, A.K.; Bhat, S.V.; Parashar, S.; Raju, A.R.; Rao, C.N.R. An electron paramagnetic resonance study of phase segregation in $Nd_{0.5}Sr_{0.5}MnO_3$. *J. Magn. Magn. Mater.* **2004**, *279*, 91–102. [CrossRef]

49. Abragam, A.; Bleaney, B. *Electron Paramagnetic Resonance of Transition Ions*; Oxford University Press: Oxford, UK, 2012; ISBN 9780199651528.

50. Weil, J.A.; Bolton, J.R.; Wertz, J.E. *Electron Paramagnetic Resonance: Elementary Theory and Practical Applications*; John Wiley & Sons, Interscience: Hoboken, NJ, USA, 1994; Volume 113, ISBN 0471572349.

51. Kittel, C. On the theory of ferromagnetic resonance absorption. *Phys. Rev.* **1948**, *73*, 155–161. [CrossRef]

52. Dijkstra, J.; Weitering, H.H.; Van Bruggen, C.F.; Haas, C.; De Groot, R.A. Band-structure calculations, and magnetic and transport properties of ferromagnetic chromium tellurides (CrTe, Cr_3Te_4, Cr_2Te_3). *J. Phys. Condens. Matter* **1989**, *1*, 9141–9161. [CrossRef]

53. Dyck, J.S.S.; Drašar, Č.; Lošt'ák, P.; Uher, C. Low-temperature ferromagnetic properties of the diluted magnetic semiconductor $Sb_{2-x}Cr_xTe_3$. *Phys. Rev. B Condens. Matter Mater. Phys.* **2005**, *71*, 115214. [CrossRef]

54. Huber, D.L.; Alejandro, G.; Caneiro, A.; Causa, M.T.; Prado, F.; Tovar, M.; Oseroff, S.B. EPR linewidths in $La_{1-x}Ca_xMnO_3$ 0 < x < 1. *Phys. Rev. B* **1999**, *60*, 12155–12161. [CrossRef]

55. de Biasi, R.S.; Gondim, E.C. Use of ferromagnetic resonance to determine the size distribution of γ-Fe_2O_3 nanoparticles. *Solid State Commun.* **2006**, *138*, 271–274. [CrossRef]

56. Vargas, J.M.; Zysler, R.D.; Butera, A. Order-disorder transformation in FePt nanoparticles studied by ferromagnetic resonance. *Appl. Surf. Sci.* **2007**, *254*, 274–277. [CrossRef]

57. Yalcin, O. *Ferromagnetic Resonance—Theory and Applications*; InTech: Rijeka, Croatia, 2013.